WPMST1-PR(17) 18139

M Lampert et al.

2D scrape-off layer turbulence measurement using Deuterium beam emission spectroscopy on KSTAR

Preprint of Paper to be submitted for publication in
Physics of Plasmas

This work has been carried out within the framework of the EUROfusion Consortium and has received funding from the Euratom research and training programme 2014-2018 under grant agreement No 633053. The views and opinions expressed herein do not necessarily reflect those of the European Commission.

2D scrape-off layer turbulence measurement using Deuterium beam emission spectroscopy on KSTAR

M. Lampert, S. Zoletnik
Wigner RCP, HAS, Budapest, Hungary

J.G. Bak, Y. U. Nam and the KSTAR team
National Fusion Research Institute, Daejeon, Korea

Intermittent events, called blobs, in the scrape-off layer of magnetically confined plasmas contribute significantly to the particle and heat loss across the magnetic field lines. Due to the low density and open magnetic field surfaces only few diagnostics can measure in the scrape-off layer. Deuterium beam emission spectroscopy (BES) is widely used for edge and core turbulence, and edge density profile measurements, however, its scrape-off layer measurement capabilities haven't been investigated yet. In this article the scrape-off layer measurement possibilities of the two dimensional KSTAR (Korea Superconducting Tokamak Advanced Research) Deuterium BES system are presented. A method is described for removing the oscillations caused by beam fluctuations. After this pre-conditioning of BES data, blobs and holes are analyzed in an L-mode and an H-mode shot with statistical tools and conditional averaging. The birth-zone of blobs and holes are identified. The main parameters of these intermittent events are calculated from conditional averaged signals, such as poloidal and radial size, and poloidal and radial propagation velocity. The BES measurements were compared to probe measurements showing that despite the low noise level of the probe measurements, beam emission spectroscopy on KSTAR is more capable of measuring intermittent structures around the separatrix and in the plasma edge. The results presented here show that beam emission spectroscopy can measure blobs and holes in two dimensions for the entire plasma shot in the plasma edge and in the scrape-off layer, as well.

I. INTRODUCTION

One of the key challenges to successful fusion energy production is understanding the anomalous cross-field transport in tokamak plasmas, that is heat and particle transport rates exceeding neoclassical predictions based on single particle motions. There is now agreement that anomalous transport is caused by plasma turbulence which contributes considerably to particle and energy loss, thus to the confinement, as well. According to observations turbulent transport in the scrape-off layer (SOL) is intermittent, it mainly contains rare individual events [1]. These events are called blobs due to their shape perpendicular to the magnetic field. They are also called filaments due to their elongation along the magnetic field. According to measurement results, blobs are formed at the position of the steepest pressure gradient at the low-field side edge [2], however, the exact source of the blob formation is still under investigation[1]. They extend along the magnetic field lines and they are propelled radially outwards by the $E \times B$ force due to charge separation driven by the curvature and the gradient of the magnetic field. This phenomenon was observed on all kinds of plasma devices including tokamaks [3][4][5][6], stellarators [7][8] and even linear or toroidal plasma devices [9] [10] [11]. It was found, that blobs large enough have higher lifetime to travel radially outwards to the point of reaching the wall which could lead to considerable wall erosion [12][13]. This aspect also rises interest to study the blobs in detail.

Detailed modeling was performed with the ESEL (edge-SOL electrostatic) code [14] in order to understand scrape-off layer physics in more detail. MAST and TCV probe measurement results were compared with simulations with the ESEL code [15][14] and good agreement was found in the statistical characteristics of the SOL turbulence in L-mode plasmas. However, high confinement mode results does not show good agreement with the ESEL simulation. Hence, a new code, HESEL (Hot edge-SOL electrostatic) is being developed to cope with high temperature regimes which also takes the changes in ion pressure into account. [16].

Due to the low temperature of the scrape-off layer, blobs can be measured with Langmuir probes. The measurement can provide density, temperature and potential fluctuations, as well. However, the time interval of the measurement in the near SOL is limited to avoid damage to the probes via the high heat load. In high performance discharges it is even impossible to measure around the origin of the blobs. Due to the simplicity of the measurement and its low noise, this technique is widely used for scrape-off layer fluctuation measurement on numerous plasma devices around the world [3][4][5]. However, usually there are only a limited number of probes available in one experiment and their arrangement is limited to few single points or one dimensional arrays.

Gas puff imaging (GPI) can provide meaningful information on blob dynamics by measuring visible light emitted during the plasma - gas interaction with a fast camera [17]. This method suffers from spatial smearing due to the

large extent of the injected gas and due to the large magnetic shear around the separatrix it is not always possible to measure the gas puff along the magnetic field lines which would provide optimal resolution. Furthermore, gas imaging signal is strong enough only with local gas injection which is often in conflict with plasma fueling.

Earlier measurements showed that Lithium beam emission spectroscopy (Li-BES) is also capable of SOL turbulence measurements [18][19]. Li-BES utilizes a diagnostic non-perturbing Lithium beam for measuring the edge and SOL electron density fluctuations and profiles by measuring the Li_{2p-2s} line emission resulting from beam excitation by the plasma. Li-BES provides low background one dimensional electron density measurement in the SOL and at the very edge, however, penetrating the plasma deeper is not possible due to the strong beam attenuation.

Deuterium beam emission spectroscopy (DBES) measures the Doppler-shifted Deuterium Balmer-alpha line (656.1 nm) emitted by a high-energy atomic beam excited by the plasma. By assuming negligible beam attenuation and constant beam profile in the SOL and at the plasma edge, BES light intensity can be considered as a proxy for electron density. The measurement usually utilizes the heating beam present on many fusion devices, thus only an observation system needs to be installed and no additional diagnostic beam is needed. Due to the wide beam (10-30 cm) the DBES measurement can provide high frequency two dimensional fluctuation measurement from the scrape-off layer to the core of the plasma. This technique would be therefore ideal for studying blob generation and propagation in any plasma discharge. However, there are few limitations which hinder this application. One is that most DBES setups are optimized for the core so as the observation lines are parallel to local magnetic field lines. Due to the different field line inclination in the SOL-edge region the resolution is not optimal. The second problem is that towards the edge the observation direction relative to the beam tends to be more perpendicular. This reduces Doppler-shift and makes the separation between the much stronger edge D_α and the beam emission difficult. The third problem arises due to the finite lifetime of the excited atomic states in the beam. Combined with the high velocity of the heating beam, spatial smearing is introduced to the measured DBES signal, which makes the measurement non-local [20][21]. Low light intensity causes further difficulties, however, with careful consideration of the photon and electronic noise and with the use of cross-correlation and cross-power techniques, one can extract meaningful information from even sub-noise signal levels.

The DBES diagnostic on the KSTAR (Korea Superconducting Tokamak Advanced Research) tokamak [22] addresses most of the above problems therefore it is a possible diagnostic for SOL turbulence measurements. The aim of this paper is to present experimental evidence for this application and to show some new observations on the origin and 2D movement of blobs in the KSTAR tokamak. Methods for the correction of the smearing effect mentioned above are considered[19] but will be presented in a separate paper.

The rest of the paper is organized as follows. The experimental setup of the KSTAR Deuterium beam emission spectroscopy is briefly described in Section II. Section III describes the fluctuation characterization of an L-mode shot by analyzing skewness and kurtosis profiles and conditional averaged signals. Section IV presents the results of H-mode SOL fluctuation analysis. Section V compares the results to probe measurements on KSTAR. The last section (Sec. VI) summarizes the results presented in this paper.

II. SCRAPE-OFF LAYER BEAM EMISSION SPECTROSCOPY MEASUREMENTS ON KSTAR

KSTAR is a fully superconducting tokamak fusion device located in Daejeon, South Korea. It has a major and minor radius of 1.8m and 0.5m, respectively. The maximum magnetic field is 3.5T and the maximum plasma current is 1MA. KSTAR is equipped with 3 neutral beams in one beam box with a beam energy of 100keV each and a total power of 5MW. The three heating beams are injected co-current from the L-port, as it can be seen in Fig. 1.

A. The KSTAR BES system

During the design of KSTAR a port was allocated for beam emission diagnostics, thus after careful design a DBES diagnostic was installed in 2012 [22]. The system measures the Doppler-shifted Deuterium alpha line with two cameras simultaneously. A CMOS camera (PhotonFocus MV1-D1312(IE/C)-G2) provides relatively slow (100Hz) but high spatial resolution (1.3 Megapixel) overview of the beam for the entire low field side. Its image can be used for spatial calibration purposes, as well

An avalanche photo-diode (APD) based camera (Fusion Instruments APDCAM-10G-4x16) is used for fast temporal (2MHz, 12bit resolution) but low spatial resolution (4 x 16 pixel, 1cm optical resolution vertically and horizontally) fluctuation measurement. The spatial position of the measurement can be adjusted vertically (from -10cm to +10cm) and radially (from r/a=0.3 to r/a=1.1). Furthermore, the APDCAM can be rotated along its axis to have horizontal and vertical detector alignment. In this paper measurements are presented where the APD matrix was oriented close to horizontal with 16 radial channels covering the SOL and edge region (see Fig. 1b and 1c). The measurement

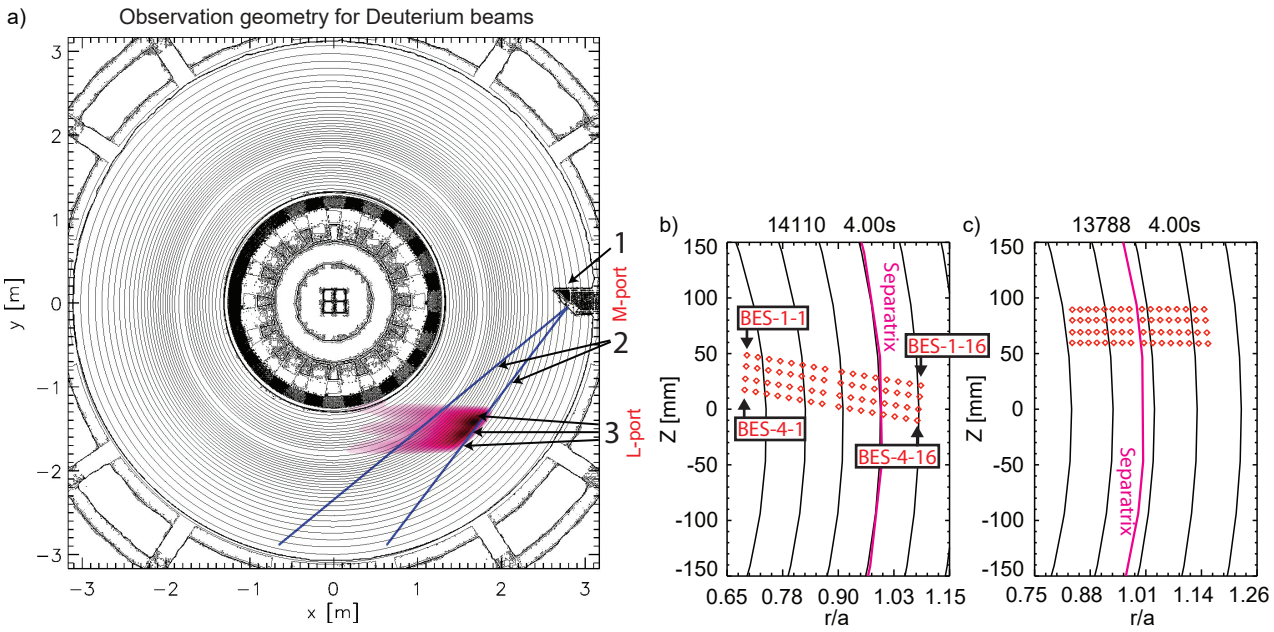

FIG. 1: a) Top view of the KSTAR BES observation geometry; 1) M-port window, 2) Field of view, 3) Deuterium beams (NBI); b) Observation geometry for the L-mode 14110 shot along with the EFIT reconstruction and the BES channel naming; c) Observation geometry for the H-mode 13788 shot along with the EFIT reconstruction

geometry can be seen in Figure 1 along with the heating beams and the BES line of sight. Furthermore, the figure also shows the spatial position of the APDCAM pixels for two shots (one L-mode shot in Fig. 1 b) and one H-mode shot in Fig. 1 c)) along with the magnetic flux surfaces and the channel naming convention. Localization of the measurement comes from the intersection of the beam with the line of sight. Although the observation direction is ideal for edge-core measurements modeling using the RENATE code [23] indicated that in the SOL both the radial and poloidal resolution is between 2 - 3 cm. This resolution depends on the number of ion sources activated in the beam, being worse for 3-source operation. This geometrical spatial smearing is comparable to the smearing due to atomic physics effects and allows measurement of at least larger blobs. An unfolding technique is being developed which takes both effects into account in order to improve the spatial resolution of the measurement. Due to space limitations this method will be presented in a separate paper.

Background light can hinder BES measurements, because only the light coming from the beam-plasma interaction can be directly related to the local electron density (and beam density), other sources represent different physical quantities, potentially also from different locations. For the KSTAR BES system, the Doppler-shift is positive and the beam light wavelength is around 660nm depending on the measurement position and beam energy. The unshifted edge Deuterium alpha radiation at 656.1nm is magnitudes brighter than the Doppler-shifted Deuterium alpha line, thus it needs to be suppressed as much as possible with careful filtering. Carbon II line radiation at 658.3nm is much weaker, but could cause significant background, as well, due to its proximity in wavelength to the beam light. After detailed modeling an interference filter was designed with 2nm bandwidth and 660.7nm central wavelength which effectively suppresses the background below 5% level even at the plasma edge (see Fig. 7 where the beam was modulated). A detailed description of the filter design can be found in [22].

B. Data conditioning

Since DBES measures the Balmer-alpha line radiation from beam atoms excited by the plasma, oscillations present in the beam current itself will be seen in the signal. Thus, the signal has to be analyzed prior to identifying any beam oscillations. Two high amplitude peaks were found in the power spectra, one at 120Hz and one at 5kHz. The former is coming from the rectifier of the high voltage power supply while the latter is an effect of the switching high voltage power supply. A method was developed in order to subtract the oscillations from the signals prior to the blob analysis. The 120Hz oscillation is not corrected for because the blobs do not contribute to the frequency range under few hundred Hertz. However, the method could be used to subtract the 120Hz oscillation if needed.

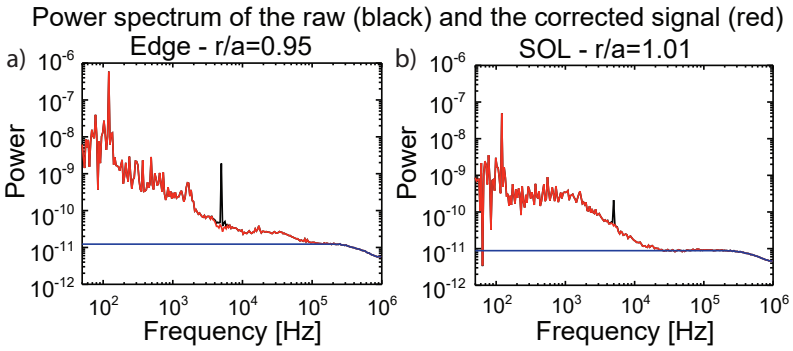

FIG. 2: Power spectra of BES signals for shot 14110 time range [3.0s, 3.5s] with (red) and without (black) the oscillation subtraction for a) edge and b) scrape-off layer. The blue graphs depict the estimated noise spectra.

The subtraction method works as follows. The method first calculates the average of signals from the 16 innermost BES channels measured at the top of the pedestal where blobs are not present. At this location the density fluctuation amplitude is low and mostly uncorrelated or out of phase between channels in a 4×4 cm area therefore the local turbulence effect is averaged out by summing up many channels. The beam current oscillations are in phase between all channels, therefore they are present in the averaged signal. The presence of a strong mode could hinder the subtraction, however, for the analyzed shots there was no mode present in the subtraction frequency range. For the 5kHz subtraction the resulting signal is filtered with a finite impulse response (FIR) filter between 4.5kHz and 5.5kHz. However, the beam oscillation amplitude is different from channel to channel. Hence, the averaged signal is subtracted from each channel after dividing it with a weighting factor, which is calculated from the power ratio of the 5kHz peak in the average signal and the signal to be corrected. The result of an oscillation subtraction can be seen in Figure 2 for a SOL and an edge BES channel for shot 14110 for time range [3.0s, 3.5s]. One can see that the peaks at 5kHz are removed while the other parts of the spectra are not effected. The estimated noise spectrum is also shown in the plots which is coming from photon and electronic noise. Electronic noise dominates in the SOL channels where the signal amplitude is low, while deeper in the plasma at higher signal levels photon statistical noise has a significant contribution [22].

III. FLUCTUATION CHARACTERIZATION OF AN L-MODE SHOT ON KSTAR

A stationary long L-mode KSTAR shot (14110) was selected for preliminary blob analysis. The plasma shot used $B_T = 2T$ toroidal magnetic field and the plasma current was $I_p = 417kA$ while the line integrated electron density was $2 \cdot 10^{19} m^{-2}$ $(n/n_{Greenwald} = 0.39)$. Only the middle NBI (NBI_A) source was operating with 0.9MW power and 70kV acceleration voltage. A BES signal measured by the APDCAM can be seen in Fig. 3a. The signals were filtered for $[1kHz, 50kHz]$ frequency range with FIR filtering and the 5kHz oscillation was subtracted with the aforementioned method. SOL fluctuations are only present in this frequency range, as one can see in Fig. 2 b). The power spectrum of the fluctuation in the plasma edge can be seen in Fig. 2 a)

In order to determine the poloidal velocity of turbulence at different radial locations the cross-correlation functions were calculated between each poloidally neighboring channels (eg. between BES-2-8 and BES-3-8). The average correlation function is calculated from the resulting three cross-correlation functions. A parabolic function is fit on the highest 3 points of the average cross-correlation function and the maximum location gives the average time lag between poloidally neighboring channels. The time lag profile is inverse proportional to the apparent poloidal velocity profile. Since a shear layer is expected to be present at the separatrix, one can determine its position by finding the position of the time lag sign change. The position can be seen in Fig. 3 b) and the result is $R_{sep} = 2230mm$. From the EFIT equilibrium reconstruction the separatrix is at $R_{sep,EFIT} = 2238mm$. This agrees with the BES result within the spatial resolution (10mm) of the BES measurement. The result shows that poloidal propagation is in the ion diamagnetic direction in the SOL and in the electron diamagnetic direction in the plasma edge, as one would expect. By looking towards the core, the BES measurement loses its sensitivity and the time lag is dominated by time lags of the background signal. In the plots the position of the separatrix is shown from the poloidal velocity profile change, however, the normalized minor radius radial scales of the plots are calculated from the EFIT reconstruction. That is why a slight discrepancy is present between the radial axis and the separatrix position.

Fig. 3 c) shows the uncalibrated light profiles for each detector row. This means that neither optical vignetting, nor filter transmission effects are corrected in the analysis. This is due to lack of calibration gas shots on KSTAR for

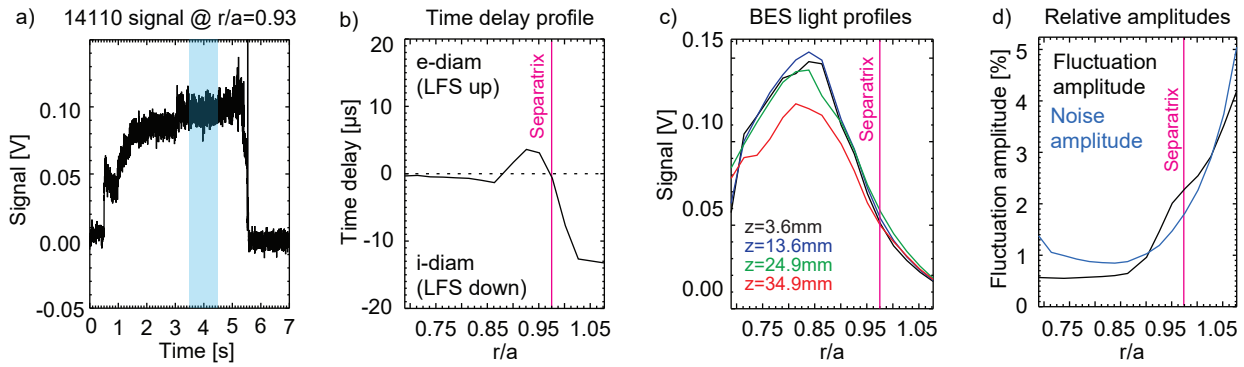

FIG. 3: a) Raw signal for shot 14110 at r/a=0.93 (the blue area is the analyzed time range); b) Radial profile of time delays between poloidally neighboring channels showing the position of the separatrix (pink) c) BES light profiles showing the pedestal and SOL region; d) Relative fluctuation and noise amplitudes for shot 14110 at time range [3.5s, 4.5s] filtered for [1kHz,50kHz]. The normalized minor radii were calculated from EFIT.

NBIs. Nevertheless, the data are usable for fluctuation analysis, since optical vignetting and filter affects mostly the edges of the profiles and the focus is on the relative fluctuations in the signals not their absolute amplitudes. One can identify the edge and the scrape-off layer region in this plot. The fluctuation and noise amplitudes were calculated for this time range, as well (see Fig. 3 d)). One can see that the relative fluctuation amplitude remains over the noise amplitude close to the separatrix and it is in the range of 1-3. Furthermore, one can see that the relative fluctuation amplitude is significantly lower than in the case of probe measurements on other machines [24][14]. This behavior is discussed in Sec. V.

After the preliminary signal processing the skewness and kurtosis profiles were calculated. The skewness is the normalized third moment of a dataset $\mathbf{X}$ and it measures the asymmetry of a signal (see Eq. 1).

$$\gamma = \mathbf{E}\left[\left(\frac{\mathbf{X}-\mu}{\sigma}\right)^3\right] \tag{1}$$

where γ is the skewness, μ is the expected value and σ is the standard deviation.

If the data have normal distribution, then their skewness is zero. If the distribution of the data has positive tail then the skewness is positive and if it has negative tail then the skewness is negative.

Kurtosis is the fourth moment of a dataset and it measures the tailedness of a dataset (see Eq. 2).

$$Kurt[\mathbf{X}] = \frac{\mathbf{E}[(\mathbf{X}-\mu)^4]}{(\mathbf{E}[(\mathbf{X}-\mu)^2])^2} - 3 \tag{2}$$

From Eq. 2 the kurtosis of a dataset with Gaussian distribution is 0. If the kurtosis is negative, then there are fewer and less extreme outliers (eg. uniform distribution). If its value is positive, then there are more and bigger outliers (eg. Laplace distribution). These functions are useful for characterizing the intermittency of the measured BES signal. The results of the skewness and kurtosis calculation for shot 14110 at time range $[3.5s, 4.5s]$ can be seen in Figure 4.

As one can see in Fig. 4 a), the skewness is positive outside the separatrix and at the edge of the plasma. By going towards the core, a steep drop can be seen in the skewness at around $r/a = 0.93$. This region is believed to be the birth zone of blobs and holes [25]. Earlier research showed, that blobs are born few centimeters inside the separatrix [26] and the skewness becomes negative in this area. The region of holes is expected to be few centimeters towards the core from the blob birth zone. In Fig. 4 a) as one goes further inside, the skewness continues to be around zero and for some channels it even drops below zero. Due to the finite lifetime of the atomic states during the beam-plasma interaction the BES signal is smeared radially inwards. This could cause masking of the holes by the larger blobs which can be one reason for the lack of negative skewness. Furthermore, as one goes inwards, the noise starts to dominate the signal (see Fig. 3) of which skewness is zero. Figure 4 b) depicts the kurtosis profiles for shot 14110 and time range $[3.5s, 4.5s]$. The tendency of the kurtosis profile is contradictory. One would expect higher kurtosis by going radially outwards as the lifetime of bigger blobs are higher and there are more extreme outliers. This is not yet fully understood.

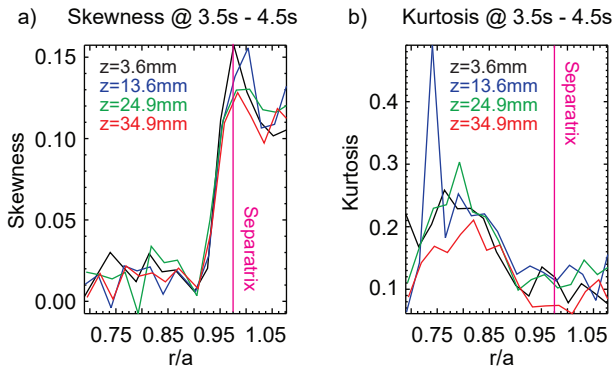

FIG. 4: Skewness (a) and kurtosis (b) profiles for shot 14110 at time range $[3.5s, 4.5s]$. The different vertical channel arrays are depicted with different colors.

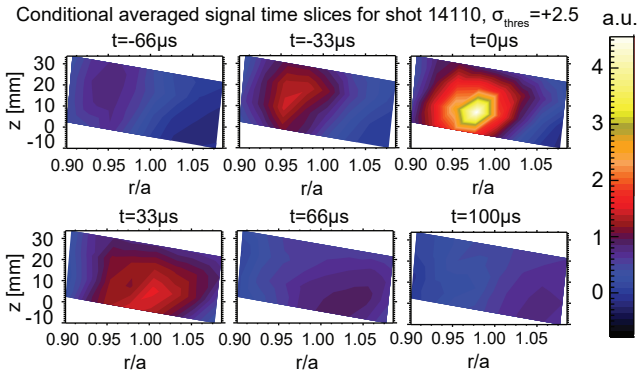

FIG. 5: Time slices of conditional average signals for shot 14110 time range of $[3.5s, 4.5s]$. The blob events were found with the $A_{cond} = +2.5 \cdot \sigma$ amplitude condition at r/a=0.98.

A. Conditional averaging

One of the feasible methods for blob and hole analysis is conditional averaging. Events are chosen based on a certain predefined condition and their signals are averaged in a defined time window. If the events are found based on the condition for one channel and the average is calculated for that channel only, then the method is called auto-conditional average. Otherwise, if the conditional average is calculated for all channels based on events found in one channel, then the result is called cross-conditional average [27]. A condition can be for example a threshold value for the signal amplitude. If that is exceeded, an event is registered at a well defined time point (eg. maximum of the signal in the time window). The threshold value is mostly chosen to be several times the standard deviation of the signal calculated for the whole time range where the events are being searched.

Our cross-conditional analysis used $A_{cond} = +2.5 \cdot \sigma$ amplitude threshold as the condition for the blobs and the time window was chosen to be $\pm 400\mu s$ around the maximum of the signal. The chosen reference channel is located at $R = 2230mm$ (r/a=0.98, close to the separatrix) because the blob birth zone is expected to be just inside the separatrix. The signal was filtered for the frequency range of $[1kHz, 50kHz]$ with FIR filtering. The calculation results a 3D quantity and it depicts the average shape and time evolution of the blobs for the given condition. Each time slice of the result depicts the shape of the blob at different times relative to the reference time. Such frames can be seen in Figure 5.

As one can see in Fig. 5 a relatively large average blob event is captured by the conditional averaging. The average blob is first seen at approximately $r/a = 0.95$, 25mm inside the separatrix. Then it moves downwards in the ion diamagnetic direction and outwards in the radial direction while its radial size increases. It is not clear whether this shape change represent the blob dynamics or, to some extent, caused by radial smearing due to beam atomic physics processes. The radial velocity of the blob is $v_{rad} \approx 300m/s$ while its poloidal velocity is $v_{pol} \approx 225m/s$. The poloidal size of the blob is around 20mm while its radial size is changing from 20mm to 40mm whilst propagating radially outwards. The movement probably continues in the far SOL, as well, however our range of measurement is limited

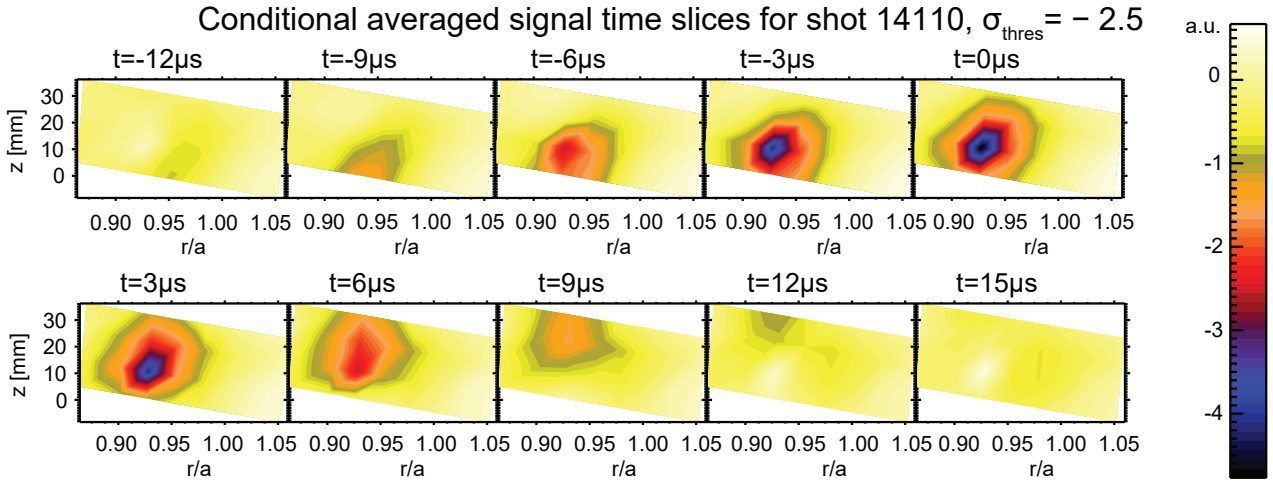

FIG. 6: Time slices of conditional average signals for shot 14110 time range of [3.5s, 4.5s]. The hole events were found with the $A_{cond} = -2.5 \cdot \sigma$ amplitude condition. (The radial range is shifted compared to Fig. 5)

and cannot observe the entire SOL. During the analysis the blob generation rate was $576 s^{-1}$.

Conditional averaging was also performed with negative threshold in order to find the holes in the signals. The reference channel was moved slightly inwards, to $r/a = 0.93$, where holes are more likely to be found. The condition for finding the holes was $A_{cond} = -2.5 \cdot \sigma$ while the time window remained the same $\pm 400 \mu s$ around the peak of the signal. The data was filtered for the same $[1kHz, 50kHz]$ range as for the blobs. The results of the calculation can be seen in Fig. 6.

As one can see conditional averaging captured a relatively large average hole event with radial and poloidal size of approximately 20mm. The hole is moving slightly radially inwards and it propagates poloidally in the electron diamagnetic direction unlike the blob, which propagates outwards in the radial direction and poloidally in the ion diamagnetic direction. However, the lifetime of the hole is much shorter than the blob's, it is in the range of several $10 \mu s$ while the blob lives longer than $100 \mu s$. The poloidal velocity of the hole is $v_{pol} = 1 km/s$ (e-diam) while its radial velocity is $v_{rad} = -400 m/s$. The average hole is born approximately at the same position where the average blob is first seen. During the analysis of the 1s long time window, the hole generation rate was $796 s^{-1}$.

One can ask the question how does the conditional averaging technique depend on the reference channel. Thorough analysis was performed in order to find the limitations of the technique. Calculations were performed with different reference channel settings from r/a=0.8 to r/a=1.03. No blob events were registered in the channels closer to the core plasma. By setting the reference to different channels in the plasma edge and the SOL where blobs are present the same conditional averaged signal was the result independent of the reference channel. The only difference was the shifted time lag due to the radial and poloidal movement of blobs.

The reference channel of the conditional averaging was also set to different ones for hole analysis. No clear indication was found for holes when the reference channel was set to channels towards the core. However, apparent holes were found in the SOL region. These hole artifacts were shadows of large blobs in that region. The shadowing effect was created by the FIR filtering, which caused negative peaks before and after the blobs due to filtering oscillation. These were found to be holes by the conditional averaging. By setting the reference channel to BES channels inside the blob birth place, the shadowing effect became negligible. In conclusion the same blobs were seen outside $r/a = 0.95$ while real holes were detected only for $0.90 < r/a < 0.95$.

IV. ANALYSIS OF H-MODE BLOB AND HOLE DYNAMICS

A feasible plasma scenario for a future energy production plasma reactor could be the H-mode. According to earlier research, H-mode plasmas have suppressed edge turbulence and steep pressure gradient in the edge transport barrier [28]. Intermittent events were also observed in the SOL of H-mode plasmas and their dynamics were analyzed on different fusion experiments [7][26].

A relatively long H-mode shot (13788) was chosen for the H-mode analysis. The toroidal magnetic field of the shot was $B_T = 1.8T$, the plasma current was 639kA and the line integrated density was $2.74 \cdot 10^{19} m^{-2}$. The shot utilized the first and the second NBI ion sources which resulted in a neutral beam heating of 2.77MW. The energy of the

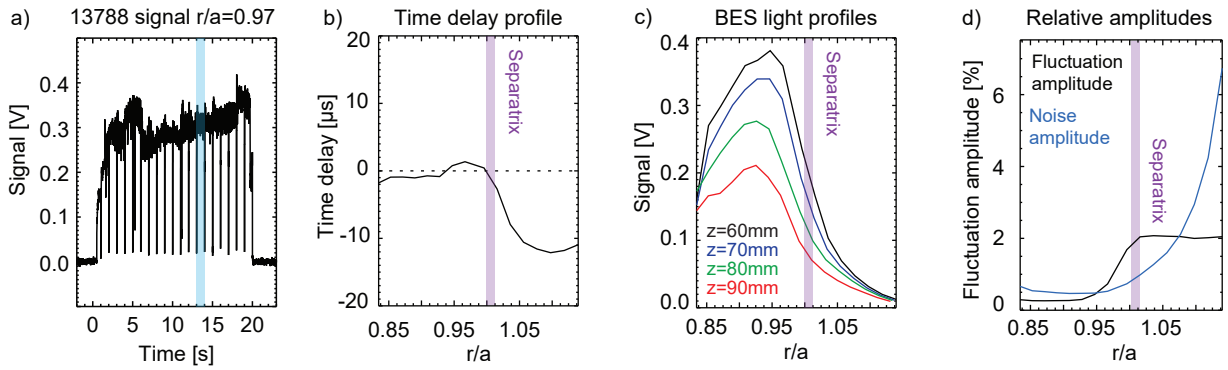

FIG. 7: (a) Raw signal for shot 13788 at r/a=0.97 (the blue area is the analyzed time range); b) Time delay profile of the shot for time range [13s,14s], the position of the velocity change shows the position of the separatrix. c) BES light profiles showing the pedestal and SOL region; d) Relative fluctuation and noise amplitudes for shot 13788 at time range [13s,14s] filtered for [1kHz,50kHz]

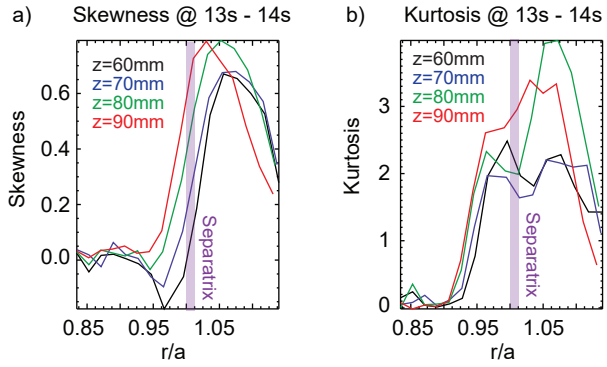

FIG. 8: Skewness (a) and kurtosis (b) profiles for shot 14110 at time range [3.5s,4.5s]. The different vertical channel arrays are depicted with different colors.

first and second ion source was 100keV and 60keV, respectively Both beams were modulated for background light measurements. The raw signal of a BES signal can be seen in Fig. 7 a).

The calculations presented hereafter are only performed for time slices between edge localized mode (ELM) bursts, since ELMs represent a strong perturbation masking blobs. The position of the separatrix was determined from the BES measurement with the same method as for the L-mode shot (see Fig. 7 b)). The radial scale of the plots is calculated from EFIT. The poloidal time-lag of turbulence is smaller, thus the poloidal velocity is larger than in the L-mode case (see Fig. 3). This is expected for an H-mode plasma where the velocity shear is stronger in the plasma edge. The separatrix is depicted as a 5mm wide area due to the curvature of the separatrix in the measurement range. As one can see, the resulting separatrix position from the time lag profile coincides with the EFIT result. Fig. 7 c) shows the uncalibrated light profiles for shot 13788 between $[13s, 14s]$ while Fig. 7 d) shows the relative fluctuation and noise amplitudes for the BES measurement filtered between [1kHz, 50kHz] for the same time interval. The results of the calculation show that the fluctuation amplitude is 2% in the SOL. The fluctuation amplitude exceeds the noise amplitude in the normalized minor radius range of $[0.95, 1.05]$. The low relative fluctuation amplitude is a result of the low spatial resolution of the BES measurement. This effect is discussed in Sec. V in more detail.

Skewness and kurtosis analysis were also performed for the H-mode measurement, as for the L-mode shot. Fig. 8 depicts the results of the calculations. The skewness profile shows similar tendency as for the L-mode shot. It is positive outside the separatrix and drops down to zero just inside the separatrix. The birth-zone of the blobs is at the position where the skewness is zero, which is approximately 1cm inside the separatrix. The skewness drops to negative values for the H-mode shot. The presence of negative skewness is expected at the position where holes are dominating, however, negative skewness was not seen in the L-mode plasma. This could be elucidated by the lower spatial smearing of the beam emission spectroscopy measurements in H-mode plasmas, thus the blobs are not smeared into the region, where holes are present. The increasing skewness radially outwards is a result of the longer lifetime

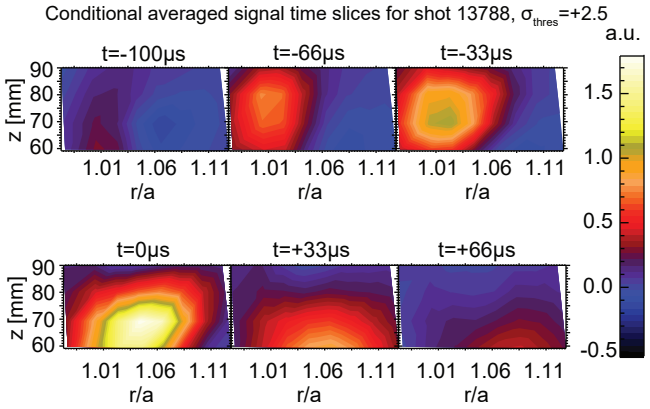

FIG. 9: Time slices of conditional average signals for shot 13788 time range of [13s,14s]. The hole events were found with the $A_{cond} = -2.5 \cdot \sigma$ amplitude condition.

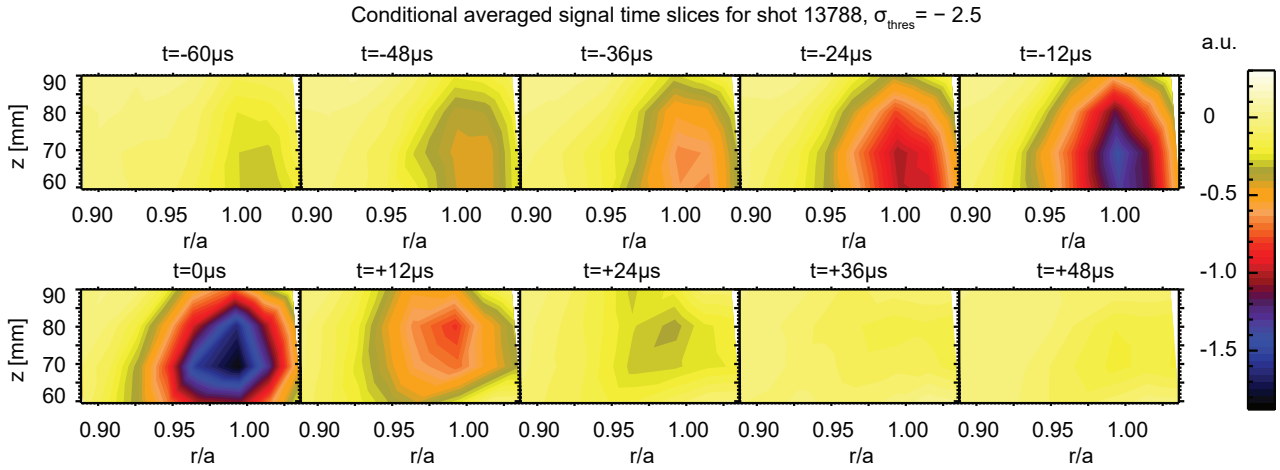

FIG. 10: Time slices of conditional average signals for shot 13788 time range of [13s,14s]. The hole events were found with the $A_{cond} = -2.5 \cdot \sigma$ amplitude condition.

of larger blobs. As one can see the skewness profiles are shifted as one goes vertically upwards. That is due to the curvature of the last closed flux surface in our measurement range. The kurtosis profile seen in Fig. 8 b) is different from the L-mode shot result in Fig. 4 d). Larger kurtosis means that there are more extreme and more frequent outliers than the Gaussian distribution. Larger blobs have higher lifetime which could explain the elevated kurtosis outside the separatrix.

Analysis of conditional averaged signal for the H-mode shot

The same analysis was performed for the H-mode shot as for the L-mode shot in terms of conditional averaging. The signal was filtered for the [1kHz, 50kHz] range with FIR filtering and a blob or a hole was registered when the signal exceeded (plus sign) or dropped below (minus sign) the $A_{thres} = \pm 2.5 \cdot \sigma$ amplitude threshold. The results of the calculations for the blobs and holes can be seen in Fig. 9 and in Fig. 10, respectively.

As one can see, the average blob in an H-mode plasma behaves similarly to the L-mode case. The blob is born just inside the separatrix, then it is propelled outwards by the $E \times B$ force. When it reaches the separatrix it is sheared by the shear layer, then it leaves our measurement range. The size of the average blob is 20mm poloidally and its radial size is changing from 20mm to 40mm during propagation. Its radial velocity is $v_{rad} \approx 200 m/s$ while its poloidal velocity is $v_{pol} \approx 150 m/s$. During the analysis 90 blob events were found in the investigated time windows, which results in a blob generation rate of $318 s^{-1}$.

The average hole dynamics in the H-mode shot is depicted in Fig. 10. As it can be seen, the average hole is born at

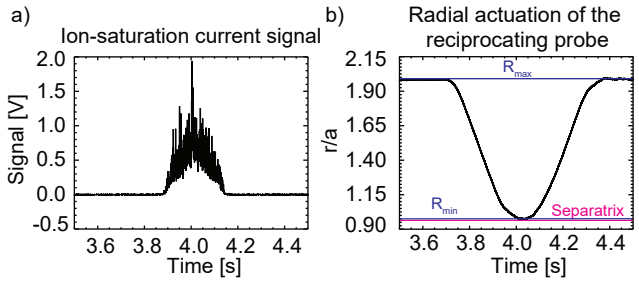

FIG. 11: a) Probe raw signal corresponding to ion-saturation current for shot 14110 in the range where the probe was reciprocating; b) Spatial calibration signal for shot 14110 for the same time range as the signal

the same position where the blob is. Its size is 20mm radially and 30mm vertically. The hole is propagating radially inwards with approximately $v_{rad} = 175m/s$ while it is moving poloidally in the electron diamagnetic direction with $v_{pol} = 166m/s$. During the analysis 150 hole events were found in the investigated time windows, which results in a blob generation rate of $530s^{-1}$.

V. COMPARISON OF BES AND PROBE MEASUREMENTS

As the most established SOL blob measurement technique is based on Langmuir probes we compare the L-mode BES results to the fast reciprocating Langmuir-probe assembly (FRLPA) [29] measurements on KSTAR. The FRLPA contains three probe tips for triple probe measurements and two tips for Mach probe measurements. Triple probe measurements can provide ion saturation current and floating potential, while the parallel velocity can be evaluated by analyzing the ion saturation currents measured by the Mach-probes. Unfortunately the ion saturation probe failed in the analyzed L-mode discharge therefore one of the Mach probe signals was analyzed and compared with the analysis of the BES data. Since the FRLPA is moving during the discharge, a spatial calibration was provided which returns the spatial position for all times during the measurement. The reciprocating movement of the FRLPA was actuated from from 3.71s to 4.36s in shot 14110, and the elapsed distance was from $R_{out} = 2638mm$ ($r/a = 2.00$) to $R_{in} = 2230mm$ ($r/a \approx 1.00$) in the inward movement. The innermost position (R_{in}) was still in the SOL, where blobs could be measured by BES. The sampling frequency for the probe measurements was 2MHz. The signal, measured with one probe tip of the FRLPA, corresponding to ion saturation current and the elapsed distance in the reciprocating movement can be seen in Fig. 11a and Fig. 11b, respectively.

During the analysis, the signal was split into equidistant time ranges, where the probe was moving 20mm, approximately the expected radial size of an average blob. The power spectrum, relative fluctuation amplitude, skewness and kurtosis were calculated for each time range. Additionally, conditional averaging was performed with $A_{cond} = +2.5 \cdot \sigma$ condition.

A calculated power spectrum in time range [3.996s, 4.090s] ($R \approx 2256mm, r/a = 1.04$) is depicted in Fig. 12 a). The fluctuations extend to about 200 kHz while a small increase is seen around 1 MHz. This latter is caused by electronic noise in the signals as it can be seen from the blue plot in Fig. 12 a). The fluctuations extend to significantly higher frequencies than the BES spectrum in Fig. 2 b). This is caused by both the larger spatial integration of the BES signal and by the higher noise level which masks the high frequency part of the BES spectrum. BES has worse spatial resolution, approximately 30mm in the SOL (considering spatial smearing from beam effects and optical imaging), while the probe size is only 3mm. Smaller events with similar poloidal and radial velocities cause higher frequency fluctuations, which are not seen in the BES measurement due to the lower spatial resolution and the spatial smearing. This aspect of the BES measurement will be addressed in a different paper in more detail.

Fig. 12 b) shows the conditional averaged signal for the same time range. Since ion saturation current measurements have low noise, low-pass filtering the signal is not necessary unlike for the BES signal. In order to subtract the trend, a 500Hz high-pass FIR filter was utilized. By fitting an exponential curve on the conditional averaged signal (see Fig. 12 b) red plots), one can find that the rising edge of the blob has $\tau_{probe,rising} = 4\mu s$, while the falling edge has $\tau_{probe,falling} = 6\mu s$ time constant. BES measurements at the same position for the same time range show longer, $\tau_{probe,rising} = 44\mu s$ and $\tau_{probe,falling} = 128\mu s$ rising and falling edge time constants, respectively. The longer time constant for BES measurement can be qualitatively understood considering the different spatial resolution of the two diagnostics, as described above. During the analysis the blob generation rate was $1050s^{-1}$ at r/a=1.03. This value is around two times higher than the one measured by BES ($576s^{-1}$), which is due to the fact that FRLPA can capture smaller events, as well.

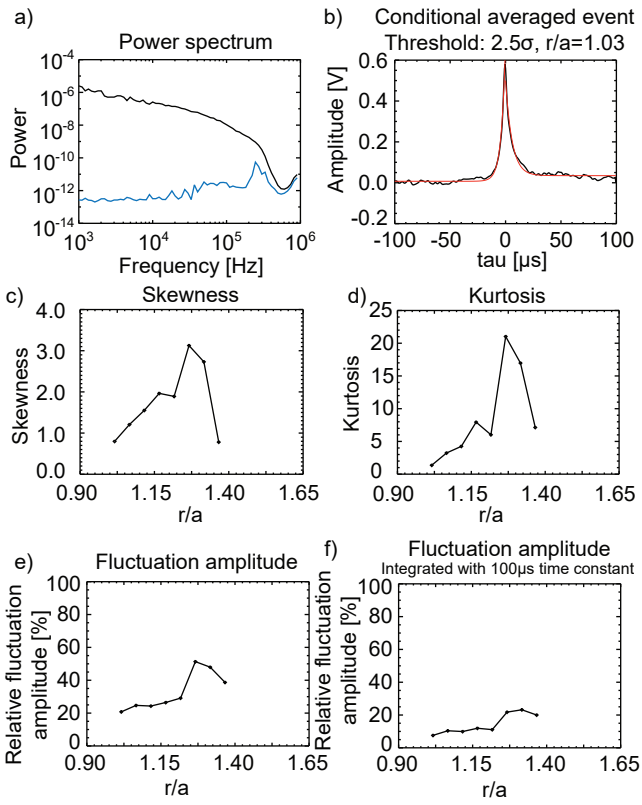

FIG. 12: a) Power spectrum for shot 14110 at [3.996s, 4.090s] ($R \approx 2256mm$) along with the noise spectrum (blue); b) Conditional average signal for shot 14110 between [3.996s,4.090s] along with the fitted exponential curves (red), $A_{thres} = 2.5 \cdot \sigma$; c) Skewness of shot 14110 for the entire measurement range; d) Kurtosis of shot 14110 for the entire measurement range; e) Relative fluctuation amplitude for the probe measurement. f) Relative fluctuation amplitude calculated with $100\mu s$ time constant integration for comparison with BES measurements.

Skewness, kurtosis and the relative fluctuation amplitude as a function of radial position were also calculated for each time frame during the inward movement and the results are shown in Fig. 12. The signals are meaningful for $r/a < 1.4$, at larger radii the fluctuation amplitude becomes comparable to the electronic noise of the measurement. In the radial range, where the signal is meaningful, the skewness is always positive in agreement with BES measurements. The value of the skewness at the probe measurements is considerably larger than in the case of BES. The reason for that is due to the significant contribution from noise in the BES measurement. The tendency of the kurtosis is in agreement with the expected behavior, thus, as one goes radially outwards kurtosis is showing increasing tendency. This is a result of the longer lifetime of larger events.

As one can see in Fig. 12 e) another significant difference between the BES and probe measurement is the much lower relative fluctuation amplitude in the BES signal. This can be understood again considering the significantly different spatial resolution of the two measurements. Using the reasoning described above at the comparison of power spectra, the BES signal should be a low-pass filtered version of the probe signal, where the filtering time constant is $\tau \approx 100\mu s$. Thus the relative fluctuation amplitude of the probe signal was calculated after integrating the signal with $100\mu s$ time constant. The resulting relative fluctuation amplitude profile can be seen in Fig. 12 f). These values are indeed closer to the level indicated by the BES measurement although they do not reach that low amplitude.

Although the above comparison indicates that the BES diagnostic capabilities are limited at small scales (and the resulting high frequencies) they offer advantages compared to probe measurements in other respect. Due to the nature of probe measurements, it is not possible to measure the entire plasma shot at different radial positions as with the BES. On KSTAR the number of reciprocating probes is 5 and hence the probe measurement lacks poloidal resolution. Furthermore, especially in H-mode, the probes can only be pushed in to the separatrix to prevent their meltdown due to high heat loads. Hence, the FRLPA cannot measure in the edge plasma and cannot reveal the hole dynamics at all. This can be also seen in Fig. 12 c) where one can see, that the skewness does not reach zero, which would show the birth zone of the blobs and holes. Since there is no indication for the birth zone, holes, which are even further inside, cannot be captured by KSTAR FRLPA measurements.

VI. SUMMARY AND DISCUSSION

Scrape-off layer and edge turbulence measurements were performed on KSTAR with Deuterium beam emission spectroscopy in different plasma scenarios. An avalanche photo-diode detector (4x16 channels) based camera provided fast (2MHz sampling) fluctuation measurements of the beam D_{alpha} line emission with 1cm radial and vertical optical resolution. The light signal fluctuations are considered as a proxy to plasma electron density modulations. During initial data analysis spurious oscillations were found in the BES signals originating from the NBI high voltage power source. An oscillation subtraction method was developed in order to remove these disadvantageous effects.

An L-mode and an H-mode shot were chosen for the aim of demonstrating the scrape-off layer turbulence measurement capabilities of the KSTAR Deuterium BES system. Main parameters of the measurements were determined such as the poloidal time lag profiles (inverse poloidal velocity profiles) and the relative fluctuation and noise amplitudes. Furthermore, the skewness and the kurtosis profiles of the shots were also investigated. It was found that the skewness profile exhibits similar behavior as it was found in other machines. The analysis showed that the birthzone of the blobs and holes are 1-2cm inside the separatrix.

In order to analyze the average behavior of blobs and holes, conditional averaging was applied. By utilizing this method, blobs and holes were found in L-mode and H-mode plasmas, as well. While blobs can be detected everythwere in the scrape-off layer, holes can only be seen at the birth location of the blobs and 1-2cm radially inwards. The poloidal and radial propagation direction of both the blobs and holes match the findings on other plasma devices: the average blob is propagating radially outward and poloidally in the ion diamagnetic drift direction, while holes are propagating radially inward and poloidally in the electron diamagnetic drift direction. The two-dimensional BES measurement suggest that the blobs change their shape as they propagate radially outward, but the contribution of beam effects is at present unclear and needs further analysis. The analysis of conditional averaging showed the generation rate of blobs and holes, as well. The generation rate was generally 50% higher for the holes in both L-mode and H-mode cases, which was seen in other machines, as well.

Probe measurements were analyzed for the same L-mode shot in order to compare probe SOL measurements to BES measurements. Probe measurements show higher relative fluctuation amplitude and higher cutoff frequency than the BES measurement. This is considered to be the effect of the limited effective spatial resolution of the BES measurement. It causes the smaller blobs to be averaged out and thus lowering the fluctuation amplitude and the cutoff frequency. This effect can be addressed quantitatively by investigating synthetic diagnostic signals which will be a subject of a different paper. Due to the limited number of probes and the lack of poloidal and radial resolution, probe measurements cannot provide detailed 2D blob measurements. Furthermore, Since probes cannot measure inside the separatrix, hole measurements are not possible with probes.

Based on the results, one can draw the conclusion that the beam emission spectroscopy diagnostic on KSTAR can provide two-dimensional scrape-off layer turbulence measurements in L-mode and H-mode plasmas for the entire plasma shot. Blob and hole dynamics can be observed and the results compare well to the same aspects of the dynamics on other machines.[26][14][24]. This continuous two-dimensional measurement capability provides an excellent possibility for detailed SOL studies. However, the downside of the diagnostic is the limited spatial resolution which prevents detection of small blob events ($< 1 - 2cm$). In order to tackle the limitation of spatial smearing, a deconvolution method is being developed, which could, to some extent, correct for the effects of the smearing and extend the diagnostic capabilities towards smaller blob events. This method and its results will be the subject of another publication.

Acknowledgments

This work has been carried out within the framework of the EUROfusion Consortium and has received funding from the Euratom research and training program 2014-2018 under grant agreement No. 633053. The views and opinions expressed herein do not necessarily reflect those of the European Commission. Financial support was also received from the National Fusion Research Institute, Daejeon, South Korea. The authors from Wigner RCP would like to thank for all the help and hospitality received from the KSTAR team during measurements and data analysis. Colleagues at Wigner RCP, HAS have also helped this work through fruitful discussions.

[1] S. Krasheninnikov, Physics Letters A **283**, 368 (2001), ISSN 0375-9601, URL `http://www.sciencedirect.com/science/article/pii/S0375960101002523`.

[2] J. R. Myra, D. A. DIppolito, D. P. Stotler, S. J. Zweben, B. P. LeBlanc, J. E. Menard, R. J. Maqueda, and J. Boedo, Physics of Plasmas **13**, 092509 (2006), http://dx.doi.org/10.1063/1.2355668, URL http://dx.doi.org/10.1063/1.2355668.

[3] J. A. Boedo, D. L. Rudakov, R. A. Moyer, G. R. McKee, R. J. Colchin, M. J. Schaffer, P. G. Stangeby, W. P. West, S. L. Allen, T. E. Evans, et al., Physics of Plasmas **10**, 1670 (2003), http://dx.doi.org/10.1063/1.1563259, URL http://dx.doi.org/10.1063/1.1563259.

[4] B. A. Carreras, V. E. Lynch, and B. LaBombard, Physics of Plasmas **8**, 3702 (2001), http://dx.doi.org/10.1063/1.1387266, URL http://dx.doi.org/10.1063/1.1387266.

[5] Y. H. Xu, S. Jachmich, R. R. Weynants, and the TEXTOR team, Plasma Physics and Controlled Fusion **47**, 1841 (2005), URL http://stacks.iop.org/0741-3335/47/i=10/a=014.

[6] S. Banerjee, H. Zushi, N. Nishino, K. Hanada, S. Sharma, H. Honma, S. Tashima, T. Inoue, K. Nakamura, H. Idei, et al., Nuclear Fusion **52**, 123016 (2012), URL http://stacks.iop.org/0029-5515/52/i=12/a=123016.

[7] G. Fuchert, G. Birkenmeier, B. Nold, M. Ramisch, and U. Stroth, Plasma Physics and Controlled Fusion **55**, 125002 (2013), URL http://stacks.iop.org/0741-3335/55/i=12/a=125002.

[8] M. Endler, L. Giannone, K. McCormick, H. Niedermeyer, A. Rudyj, G. Theimer, N. Tsois, S. Zoletnik, the ASDEX Team, and the W7-AS Team, Physica Scripta **51**, 610 (1995), URL http://stacks.iop.org/1402-4896/51/i=5/a=011.

[9] G. Y. Antar, J. H. Yu, and G. Tynan, Physics of Plasmas **14**, 022301 (2007), http://dx.doi.org/10.1063/1.2424886, URL http://dx.doi.org/10.1063/1.2424886.

[10] I. Furno, B. Labit, A. Fasoli, F. M. Poli, P. Ricci, C. Theiler, S. Brunner, A. Diallo, J. P. Graves, M. Podest, et al., Physics of Plasmas **15**, 055903 (2008), https://doi.org/10.1063/1.2870082, URL https://doi.org/10.1063/1.2870082.

[11] S. H. Mller, C. Theiler, A. Fasoli, I. Furno, B. Labit, G. R. Tynan, M. Xu, Z. Yan, and J. H. Yu, Plasma Physics and Controlled Fusion **51**, 055020 (2009), URL http://stacks.iop.org/0741-3335/51/i=5/a=055020.

[12] S. J. Zweben, J. A. Boedo, O. Grulke, C. Hidalgo, B. LaBombard, R. J. Maqueda, P. Scarin, and J. L. Terry, Plasma Physics and Controlled Fusion **49**, S1 (2007), URL http://stacks.iop.org/0741-3335/49/i=7/a=S01.

[13] D. Carralero, P. Manz, L. Aho-Mantila, G. Birkenmeier, M. Brix, M. Groth, H. W. Müller, U. Stroth, N. Vianello, and E. Wolfrum (ASDEX Upgrade team and JET Contributors and EUROfusion MST1 Team), Phys. Rev. Lett. **115**, 215002 (2015), URL http://link.aps.org/doi/10.1103/PhysRevLett.115.215002.

[14] O. Garcia, J. Horacek, R. Pitts, A. Nielsen, W. Fundamenski, V. Naulin, and J. J. Rasmussen, Nuclear Fusion **47**, 667 (2007), URL http://stacks.iop.org/0029-5515/47/i=7/a=017.

[15] F. Militello, W. Fundamenski, V. Naulin, and A. H. Nielsen, Plasma Physics and Controlled Fusion **54**, 095011 (2012), URL http://stacks.iop.org/0741-3335/54/i=9/a=095011.

[16] J. Olsen, J. Madsen, A. H. Nielsen, J. J. Rasmussen, and V. Naulin, Plasma Physics and Controlled Fusion **58**, 044011 (2016), URL http://stacks.iop.org/0741-3335/58/i=4/a=044011.

[17] S. Zweben, R. Maqueda, D. Stotler, A. Keesee, J. Boedo, C. Bush, S. Kaye, B. LeBlanc, J. Lowrance, V. Mastrocola, et al., Nuclear Fusion **44**, 134 (2004), URL http://stacks.iop.org/0029-5515/44/i=1/a=016.

[18] G. Birkenmeier, P. Manz, D. Carralero, F. Laggner, G. Fuchert, K. Krieger, H. Maier, F. Reimold, K. Schmid, R. Dux, et al., Nuclear Fusion **55**, 033018 (2015), URL http://stacks.iop.org/0029-5515/55/i=3/a=033018.

[19] S. Zoletnik, S. Fiedler, G. Kocsis, G. K. McCormick, J. Schweinzer, and H. P. Winter, Plasma Physics and Controlled Fusion **40**, 1399 (1998), URL http://stacks.iop.org/0741-3335/40/i=7/a=013.

[20] M. W. Shafer, R. J. Fonck, G. R. McKee, and D. J. Schlossberg, Review of Scientific Instruments **77**, 10F110 (2006), http://dx.doi.org/10.1063/1.2221908, URL http://dx.doi.org/10.1063/1.2221908.

[21] M. F. J. Fox, A. R. Field, F. van Wyk, Y. c Ghim, A. A. Schekochihin, and the MAST Team, Plasma Physics and Controlled Fusion **59**, 044008 (2017), URL http://stacks.iop.org/0741-3335/59/i=4/a=044008.

[22] M. Lampert, G. Anda, A. Czopf, G. Erdei, D. Guszejnov, . Kovcsik, G. I. Pokol, D. Rfy, Y. U. Nam, and S. Zoletnik, Review of Scientific Instruments **86**, 073501 (2015), http://dx.doi.org/10.1063/1.4923251, URL http://dx.doi.org/10.1063/1.4923251.

[23] D. Guszejnov, G. I. Pokol, I. Pusztai, D. Refy, S. Zoletnik, M. Lampert, and Y. U. Nam, Review of Scientific Instruments **83**, 113501 (2012), URL \url{http://scitation.aip.org/content/aip/journal/rsi/83/11/10.1063/1.4764564}.

[24] G. S. Xu, V. Naulin, W. Fundamenski, C. Hidalgo, J. Alonso, C. Silva, B. Gonalves, A. Nielsen, J. J. Rasmussen, S. Krasheninnikov, et al., Nuclear Fusion **49**, 092002 (2009), URL http://stacks.iop.org/0029-5515/49/i=9/a=092002.

[25] D. A. Russell, J. R. Myra, and D. A. DIppolito, Physics of Plasmas **14**, 102307 (2007), http://dx.doi.org/10.1063/1.2780137, URL http://dx.doi.org/10.1063/1.2780137.

[26] J. Cheng, L. W. Yan, W. Y. Hong, K. J. Zhao, T. Lan, J. Qian, A. D. Liu, H. L. Zhao, Y. Liu, Q. W. Yang, et al., Plasma Physics and Controlled Fusion **52**, 055003 (2010), URL http://stacks.iop.org/0741-3335/52/i=5/a=055003.

[27] H. L. Pecseli and J. Trulsen, Physics of Fluids B: Plasma Physics **1**, 1616 (1989), http://dx.doi.org/10.1063/1.858940, URL http://dx.doi.org/10.1063/1.858940.

[28] F. Wagner, G. Becker, K. Behringer, D. Campbell, A. Eberhagen, W. Engelhardt, G. Fussmann, O. Gehre, J. Gernhardt, G. v. Gierke, et al., Phys. Rev. Lett. **49**, 1408 (1982), URL https://link.aps.org/doi/10.1103/PhysRevLett.49.1408.

[29] J. G. Bak, S. G. Lee, J. Y. Kim, and K. P. Team, Contributions to Plasma Physics **50**, 892 (2010), ISSN 1521-3986, URL http://dx.doi.org/10.1002/ctpp.201010151.